Capacitor-embedded 0.54 pJ/bit silicon-slot photonic crystal waveguide modulator

Xiaonan Chen,[1] Yun-Sheng Chen,[1] Yang Zhao,[1] Wei Jiang,[2] and Ray T. Chen[1,*]

[1]*Microelectronics Research Center, Department of Electrical and Computer Engineering, The University of Texas at Austin, Austin, Texas 78758, USA*

[2]*Department of Electrical and Computer Engineering and Institute for Advanced Materials, Devices, and Nanotechnology, Rutgers University, Piscataway, New Jersey 08854, USA*

**Corresponding author: raychen@uts.cc.utexas.edu*

Received September 3, 2008; revised November 25, 2008; accepted December 10, 2008; posted January 15, 2009 (Doc. ID 101054); published February 24, 2009

A high-speed compact silicon modulator based on the lateral capacitor configuration is experimentally demonstrated with low-power consumption and 3 dB modulation depth. The capacitor layout is introduced to scale down the total modulator capacitance to 30×10^{-15} F, which effectively reduces the rf power consumption to 0.54 pJ/bit. Exploiting the slow group velocity of light in the slot photonic crystal waveguides, the device reported herein exhibits higher modulation efficiency than conventional capacitor modulator and provides a $V_{\pi}L$ figure of merit of 0.18 V cm at the wavelength of 1548 nm. © 2009 Optical Society of America

OCIS codes: 130.5296, 200.6715, 310.2790.

As one of the principal components required for composing silicon integrated photonic circuits, high-speed silicon modulators have continued to evolve with significant performance improvement over the past few years [1–7]. High-frequency performance and power consumption are generally considered among the most important characteristics of monolithically integrated silicon modulators for optical interconnects [7]. One of the most widely employed modulation mechanisms is based upon free-carrier electro-optic (EO) effect [8] induced by carrier injection and extraction in the intrinsic region of a forward-biased silicon p-i-n diode device [5,7]. The modulation speed of charge-injection-based silicon modulators is limited by the slow recombination dynamics of minority carriers [9]. Capacitor-embedded silicon modulators open the opportunities for excluding the recombination lifetime limit by involving carrier accumulation process and minimizing recombination of electron-hole pairs [1]. However, the low modulation efficiency of conventional capacitor-embedded silicon modulators restricts their application in highly integrated ultracompact optical interconnect systems. As a potential solution for efficiency enhancement in active waveguide devices, photonic crystal waveguides (PCW) have shown the capability to guide light with lower group velocity and thereby improve the interaction of the light wave and the applied voltage in the active region [10]. Here we present a compact capacitor-embedded silicon modulator with ultralow power consumption by exploiting the slow-light effect in slot PCW [11].

Silicon EO modulators in highly integrated on-chip systems always require an optimum design with low power consumption [12]. It has been reported that the rf power for multigigahertz switching in a p-i-n diode modulator is higher than 5 pJ/bit, i.e., 50 mW at 10 GHz. In contrast, the rf power required by a capacitor modulator is given by $P_{\mathrm{AC}}=CV^2/2/\mathrm{bit}$ [13], where V is the voltage amplitude of an rf pulse signal. We may design a capacitor modulator with either small capacitance or ultralow driving voltage in order to minimize the ac power consumption. Photonic-crystal-based structures are capable of shrinking the device interaction length to hundreds of micrometers and the device height to hundreds of nanometers [10], which scales down the dielectric area of the lateral capacitor in a slotted waveguide and thereby significantly reduces the overall capacitance.

The silicon modulator presented here is a Mach–Zehnder interferometer (MZI) based on lateral capacitor-embedded PCW, as shown in Fig. 1(a). The waveguide comprises a p-type doped silicon photonic crystal slab with a center slot working as the vertical gate oxide. Under accumulation conditions ($V>0$), the majority carriers in the positive-x silicon region, defined in Fig. 1(a), modify the refractive index so that phase shift is induced in the optical mode. Compared with conventional capacitor-embedded silicon rib waveguides [2], the optical mode as indicated in Fig. 1(a) is more tightly confined within 1 μm perpendicular to the capacitor dielectric and thus interacts more strongly with the accumulated charges. The calculated dispersion diagram shown in Fig. 1(b) indicates slow-light effect at the band edge of the defect mode.

For accurate understanding of the carrier distribution, which determines the refractive index perturbation in the silicon PCW, the Poisson equation is solved by applying the classical model [14]. The calculated profile of the hole carriers under different driving voltages is shown in Fig. 2(a). At steady state the diffusion current due to the gradient of the hole concentration is compensated by the opposite drift current so that the total dc current is negligible. Each hole carrier profile is converted into the index change through an empirical equation of $\Delta n_h=-8.5\times10^{-18}(p-p_0)^{0.8}$ [8], as shown in Fig. 2(b). We use the plane-wave expansion method to calculate the dispersion diagram of the slot PCW with different index perturbations and derive the phase shift by $\Delta\phi_{\mathrm{PC}}=\Delta\omega_0 L/v_g$, where $\Delta\omega_0$ is the vertical shift of the dis-

0146-9592/09/050602-3/$15.00 © 2009 Optical Society of America

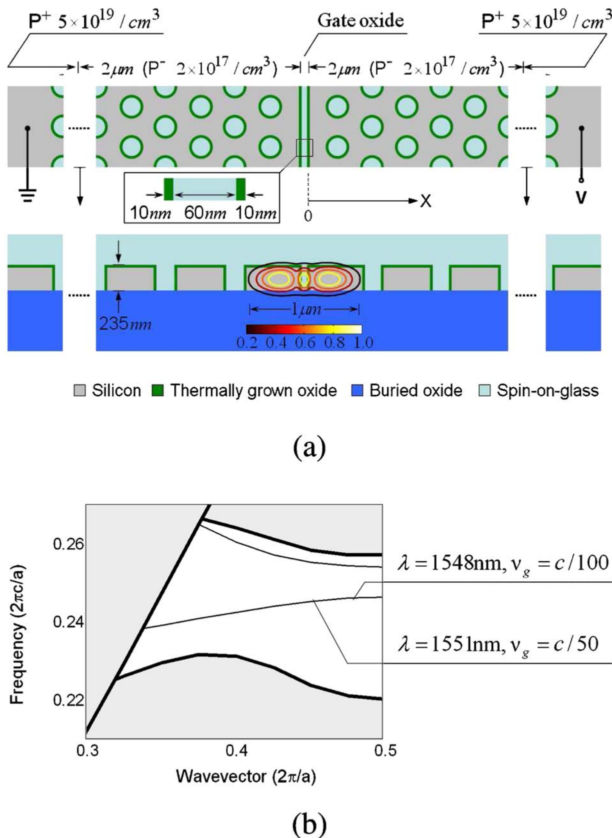

Fig. 1. (Color online) Schematics and calculation results. (a) Top and cross-sectional views of a lateral capacitor-embedded photonic crystal waveguide. The cross-sectional view shows the simulated two-dimensional field amplitude contour. (b) Dispersion diagram of the slot photonic crystal waveguide. The thick line is the light line. The thin curves indicate the defect modes.

persion curve shown in Fig. 1(b) [15] and v_g is the group velocity of the defect mode. Calculation indicates that the slot PCW-based active arm, designed to give $v_g=c/100$ with 300 μm interaction length required for inducing π phase shift, composes a compact capacitor-embedded silicon modulator with a $V_{\pi}L$ product of 0.18 V cm.

The capacitor-embedded PCW MZI modulator is fabricated on a silicon-on-insulator wafer with a 250 nm top silicon layer. The slot nanostructures are formed in a hexagonal lattice photonic crystal slab with a lattice constant $a=400$ nm and a hole diameter $d=220$ nm. The waveguide slab layer is patterned by electron-beam lithography and reactive ion etching, followed by growing thin thermal oxide up to 10 nm for surface passivation. p^- and p^+ regions are defined using photolithography and implanted to the concentration $N_A(p^-)=2\times 10^{17}$ cm^{-3} and $N_A(p^+)=5\times 10^{19}$ cm^{-3}, respectively. The contact windows are opened by a third photolithography process, and aluminum electrodes are formed by a lift-off process. As the last step, we fill the air holes and the center slot with spin-on-glass, and postbake the sample at 425°C for decarbonization [11]. The overall modulator schematic and images of the resulting device are shown in Fig. 3. A tapering mode coupler with a skew slot [16] is integrated at both ends of the slot PCW in order to relieve the mode mismatch with the strip waveguide and to maintain the electrical isolation between the two regions separated by the slot. A dummy sample without the center slot is also fabricated to measure the equivalent series resistance. The total resistance between adjacent electrodes is about 120 Ω. The compact waveguide design with the lateral capacitor layout provides significant reduction of the total capacitance from the conventional rib waveguide modulators [1,2], pushing it down to an experimentally confirmed value of 30 fF. Combined with the 120 Ω series resistance, the resistance-capacitance (RC) circuit has a time constant of 23 ps, On the other hand, the transit time for the light wave to propagate through the active region is given by $t=L/v_g=100$ ps, which indicates a 10 GHz frequency limitation for the switching bandwidth. An rf traveling-wave electrode is a feasible solution to co-propagate both the electrical and optical signals with similar speeds and thus can overcome the limitations associated with the electrical RC delay and the transit time for light propagation.

TE-polarized light at a wavelength of 1548 nm is used for dc characterization of the MZI modulator. As shown in Fig. 4(a), a maximum modulation depth of 90% is obtained at 6 V dc bias voltage. The leakage current during operation is below 200 pA, which indicates negligible dc power consumption [$P_{DC}=1.2$ nW]. It is measured that the overall optical insertion loss of the modulator is approximately

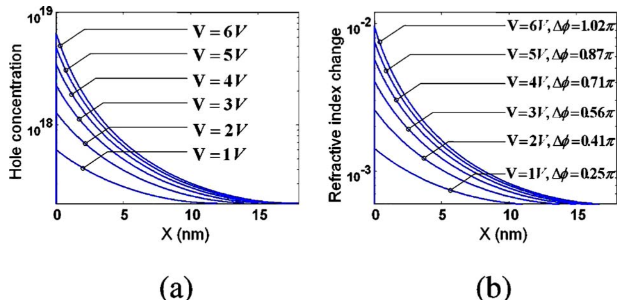

Fig. 2. (Color online) Calculated profiles of (a) the hole carriers and (b) the corresponding refractive index changes under different driving voltages.

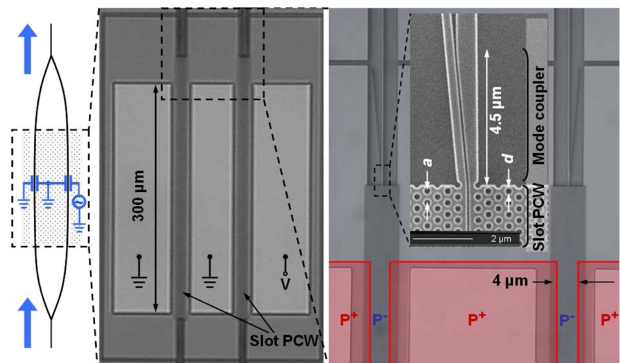

Fig. 3. (Color online) Overall modulator schematic and image of the fabricated device. Microscopic image of a capacitor-embedded photonic crystal Mach–Zehnder interferometer, where colored overlays indicate the p^- and p^+ regions. The inset is a scanning electron microscopy image of one end of the slot PCW.

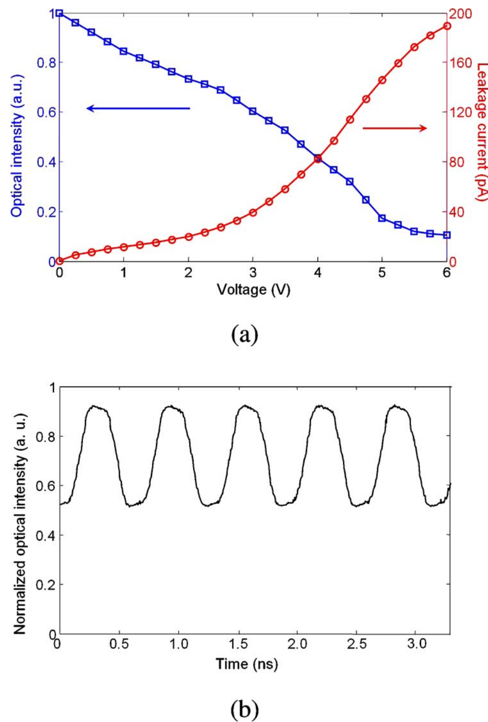

Fig. 4. (Color online) Modulation measurement results. (a) Optical intensity at the modulator output and the leakage current as a function of the static driving voltage. (b) Normalized output optical intensities of the modulator working at 1.6 Gbit/s.

−40 dB fiber to fiber, dominated by the fiber-to-strip-waveguide coupling (−13 to −15 dB/port) and the strip-waveguide-to-PCW coupling (−5 dB/port at $v_g = c/100$). It has been reported that the strip-waveguide-to-PCW coupling efficiency T is a function of the group velocity v_g as $T=3.22(c/v_g)^{-0.74}$ [10]. We make a trade-off between v_g and T in order to obtain higher output intensity so that the high-speed photodetector provides gigahertz response. The light wavelength is tuned to 1551 nm to control the group velocity around $v_g=c/50$, as indicated in Fig. 1(b) also. A square-wave electrical signal having a peak-to-peak amplitude of 6 V and a duty cycle of 50% is used for high-frequency modulation characterization. The output optical intensity of the modulator at the bit rate of 1.6 Gbit/s with 3 dB modulation depth is shown in Fig. 4(b). As a critical characteristic, the rf power consumption, given by $P_{AC}=CV^2/2/\text{bit}$, is reduced to 0.54 pJ/bit, which is one of the lowest values for any high-speed MZI silicon modulator obtained to date. The high-frequency modulation depth is limited by reduction of the group velocity and the degradation of the detector bandwidth due to low optical intensity.

In conclusion, a high-speed capacitor MZI modulator is demonstrated with ultralow power consumption of 0.54 pJ/bit, which is desirable for highly integrated on-chip applications. With the enhancement of the modulation efficiency due to the slow-light effect in PCW, the interaction length of the device is scaled down to 300 μm, which is 1 order of magnitude shorter than the most recent work based on capacitors [2]. As one benefit of the compact active region, the modulator provides a $V_\pi L$ figure of merit of 0.18 Vcm at the wavelength of 1548 nm.

This work is supported by U.S. Air Force Office of Scientific Research (AFOSR) contract FA9550-05-C-0171 monitored by G. Pomrenke. Support from Defense Advanced Research Projects Agency (DARPA), the State of Texas, and Sematech are also acknowledged. Nanofabrication and characterization facilities used for this work are partially supported by AFOSR, the National Science Foundation (NSF), and National Nanotechnology Infrastructure Network Program.

References

1. A. Liu, R. Jones, L. Liao, D. Samara-Rubio, D. Rubin, O. Cohen, R. Nicolaescu, and M. Paniccia, Nature **427**, 615 (2004).
2. L. Liao, D. Samara-Rubio, M. Morse, A. Liu, D. Hodge, D. Rubin, U. D. Keil, and T. Franck, Opt. Express **13**, 3129 (2005).
3. A. Liu, L. Liao, D. Rubin, H. Nguyen, B. Ciftcioglu, Y. Chetrit, N. Izhaky, and M. Paniccia, Opt. Express **15**, 660 (2007).
4. L. Gu, W. Jiang, X. Chen, L. Wang, and R. T. Chen, Appl. Phys. Lett. **90**, 071105 (2007).
5. Q. Xu, S. Manipatruni, B. Schmidt, J. Shakya, and M. Lipson, Opt. Express **15**, 430 (2007).
6. T. Barwicz, H. Byun, F. Gan, C. W. Holzwarth, M. A. Popovic, P. T. Rakich, M. R. Watts, E. P. Ippen, F. X. Kartner, H. I. Smith, J. S. Orcutt, R. J. Ram, V. Stojanovic, O. O. Olubuyide, J. L. Hoyt, S. Spector, M. Geis, M. Grein, T. Lyszczarz, and J. U. Yoon, J. Opt. Netw. **6**, 63 (2007).
7. W. M. J. Green, M. J. Rooks, L. Sekaric, and Y. A. Vlasov, Opt. Express **15**, 17106 (2007).
8. R. A. Soref and B. R. Bennett, IEEE J. Quantum Electron. **23**, 123 (1987).
9. C. A. Barrios, V. R. Almeida, R. Panepucci, and M. Lipson, J. Lightwave Technol. **21**, 2332 (2003).
10. Y. A. Vlasov, M. O' Boyle, H. F. Hamann, and S. J. McNab, Nature **438**, 65 (2005).
11. X. Chen, W. Jiang, L. Gu, and R. T. Chen, Appl. Phys. Lett. **91**, 091111 (2007).
12. W. Jiang, L. Gu, X. Chen, and R. T. Chen, Solid-State Electron. **51**, 1278 (2007).
13. A. Agarwal and J. H. Lang, *Foundations of Analog and Digital Electronic Circuits*, 1st ed. (Morgan Kaufmann, 2005), p. 596.
14. S. M. Sze and K. K. Ng, *Physics of Semiconductor Devices*, 3rd ed. (Wiley, 2007), p. 233.
15. Y. Jiang, W. Jiang, L. Gu, X. Chen, and R. T. Chen, Appl. Phys. Lett. **87**, 221105 (2005).
16. J. Blasco and C. A. Barrios, *Proceedings of the Conference on Lasers and Electro-Optics Europe* (IEEE, 2005), p. 607.